PHOTONICS Research

Effects of coupling and phase imperfections in programmable photonic hexagonal waveguide meshes

IMAN ZAND[1,2] AND WIM BOGAERTS[1,2,*]

[1]Photonics Research Group, Department of Information Technology, Ghent University-IMEC, 9052 Ghent, Belgium
[2]Center of Nano and Biophotonics, Ghent University, 9052 Ghent, Belgium
*Corresponding author: wim.bogaerts@ugent.be

Received 10 September 2019; revised 24 November 2019; accepted 18 December 2019; posted 18 December 2019 (Doc. ID 376227); published 31 January 2020

We present a study of the effect of imperfections on the transmission and crosstalk in programmable photonic meshes with feedback loops consisting of tunable couplers and phase shifters. The many elements in such a mesh can generate a multitude of parasitic paths when the couplers and phase shifters deviate even slightly from their nominal value. Performing Monte Carlo simulations, we show that small stochastic imperfections in the phase and coupling (<1.0%) can introduce unwanted interferences and resonances and significantly deteriorate the frequency response of the circuit. We also demonstrate that, in the presence of imperfections, the programming strategy of the unused couplers can reduce effects of such parasitics. © 2020 Chinese Laser Press

https://doi.org/10.1364/PRJ.376227

1. INTRODUCTION

Recent developments in photonic integrated circuits (PICs) technologies have enabled a wide range of research on programmable PICs for various applications such as optical communication, artificial neural networks, and quantum information technologies [1–15]. Broadband switches [1], microwave photonic subsystems [6], and universal multiport photonic interferometers (important for advanced optical functions) [3,11,12,14,16–18] are examples of recent demonstrations in this field. It is hoped that, similar to the field programmable gate arrays (FPGAs) in electronics, multifunctionality of programmable photonic circuits will enable us to considerably reduce the required time and cost to design, fabricate, and test new photonic chips.

In most programmable PIC architectures, optical signal processing tasks take place in a linear optical core consisting of a waveguide mesh, where the topology and connectivity defines the possible implementable functionalities. These meshes are normally constructed using tunable optical building blocks such as couplers/beam splitters and phase shifters, controlled by electronics. We can distinguish two main approaches to implement such meshes: "forward-only meshes" [3,9,11,12,15,16] and "meshes with feedback loops" [2,10,14,17,19–22]. In the first approach, linear optical transformations are implemented by one-way propagation from a set of input ports to a set of output ports, essentially implementing a transmission matrix (T-matrix). In most implementations, all optical paths have the same length (apart from a 0–2π phase shift), and the response is largely wavelength-independent.

In the second type of meshes, the waveguides are connected in loops that can implement differential delay lines, ring resonators, and optical feedback circuits, enabling applications such as finite/infinite impulse response multiport interferometers and RF filters [21]. In this approach, all ports can serve as inputs and outputs, and the linear optical operation is described by a wavelength dependent scattering matrix (S-matrix). These 2D waveguide meshes/lattices have much higher flexibility [2,10,14,17,19–22], as they can also be configured to function as a forward-only mesh. The first demonstration of integrated waveguide meshes with feedback loops, which had been inspired by FPGAs, was done by Zhuang *et al.* using square lattices and Mach–Zehnder interferometers (MZIs) [2]. Later, triangular and hexagonal lattices were studied by Pérez *et al.* [19]; they showed that hexagonal meshes are superior in terms of various figures of merit such as spatial tuning reconfiguration steps and reconfiguration performance.

The physical implementations of such programmable photonic circuits consist of many identical optical building blocks (phase shifters and tunable couplers), and the routing of the light is controlled by electronics and software. Such a chip, therefore, requires electronic drivers for all the optical elements, an assembly scheme for fibers and high-speed connections, and algorithms and software that will allow a designer to actually implement a useful function. Hence, there are various possible

sources of errors, both in design and fabrication, causing imperfect behavior of the optical building blocks, which in turn will introduce parasitic behavior in the mesh. These errors (acting as additional loss, phase errors, and coupling errors) can be accumulated and dramatically deteriorate the response of the circuit [18,22]. In particular, for the meshes with feedback loops, they create a multitude of secondary and tertiary paths for the light, which can cause unwanted interferences and resonances and, thus, affect the frequency response of circuit [22]. This will result in a wavelength-dependent transmission "ripple" in the desired output ports and crosstalk in the other ports.

We can discern three types of parasitics originating from the phase shifters and tunable couplers.

- Nonidealities in the optical transmission where light remains in the intended waveguide paths. This can be an error in the phase shift or an error in the coupling ratio. These, in principle, could be compensated with improved control electronics and algorithms of the tunable building blocks.
- Nonidealities in the components where light is coupled to a waveguide path, where it should never end up during normal operation. The most common example is backscattering in waveguides and backreflection/backcoupling in tunable couplers [23].
- Nonidealities that radiate light from the waveguides altogether. Due to reciprocity, such defects can also capture light radiated elsewhere on the chip, which can introduce secondary light paths.

In this paper, we focus on the first type of nonidealities and study the effect of small stochastic imperfections in the phase and coupling control of a seven-cell hexagonal mesh consisting of 2 × 2 couplers and phase shifters connected by waveguides. For the simulations, we have extended the photonic circuit simulator Caphe (part of the design framework IPKISS) [24] with models for the mesh components and performed Monte Carlo simulations to evaluate the effect of imperfections [a summary of the simulation flow is shown in Fig. 1(a)].

2. SIMULATION METHODOLOGY

As a baseline case for the simulations, we have constructed a uniform mesh based on hexagonal cells, which offer flexible programming, especially because this mesh type allows clockwise/counterclockwise coupling [19]. Figure 1(b) shows a schematic representation of a hexagonal mesh consisting of seven hexagonal cells. As seen, the arms of the 2 × 2 couplers (CPs) are connected to the phase shifters (PSs) through silicon waveguides, where optical length of the phase shifters is assumed to be zero and where they only apply the desired additional phase shifts. We also assume that perfect control over the variable property of each component is feasible, and this is over its entire operational range. This limit is 0–100% coupling efficiency for the CPs and 0°–360° phase delay for the PSs; further, all elements can be controlled independently, ignoring at this stage effects of tuning crosstalk (e.g., through thermal crosstalk). The total length of each segment is assumed to be 300 μm with a waveguide bend radius of 10 μm.

Our circuit generator is implemented using Python on top of the IPKISS/Caphe framework by Luceda Photonics, which

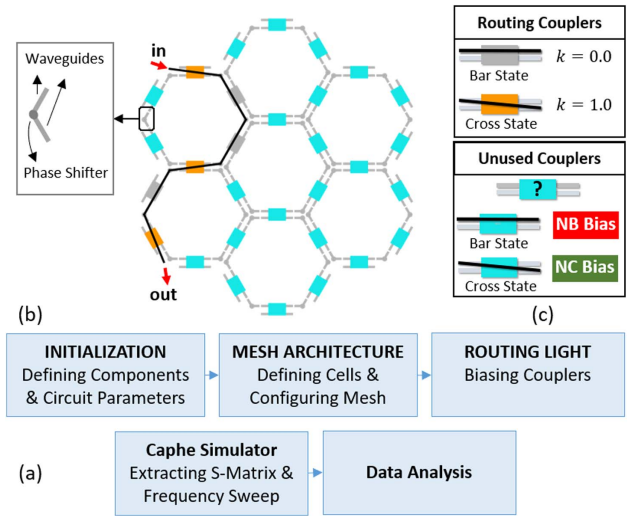

Fig. 1. (a) Summary of the simulation flow to study effects of parasitics. (b) Schematic representation of the seven-cell hexagonal mesh, where 2 × 2 couplers are connected to the phase shifters (PSs) through silicon waveguides. (c) For each mesh configuration, couplers are categorized to routing couplers (involved in defining light paths) and unused couplers (their state, in principle, does not affect the light paths). Orange and gray colors show cross and bar states of the routing couplers; unused couplers are shown only by the blue. Note that, in normal bar bias (NB bias), unused couplers are programmed in the bar state, while, in normal cross bias (NC bias), they are programmed in the cross state.

generates hexagonal lattices with arbitrary configurations of the cells. Mesh components are implemented as parametric cells in the IPKISS framework, so they contain a layout, connectivity information (netlist), and a circuit model. This means that both realistic and abstract building blocks of the components can be used for the calculations, and the generated layouts can be used for the fabrication. Also, as the layout feeds back into the circuit simulation, actual waveguide lengths and device parameters are being used. Even though the components are considered identical in the entire mesh, we can set the circuit model parameters for each instance individually to "program" the circuit. In the Caphe circuit simulator, the optical properties such as phase shift (for the PS blocks), coupling coefficient (for the CP blocks), and insertion loss (for both) can be varied. We can also visualize the model parameters for each building block as part of the overall circuit. This can be used to test programmability and also to evaluate sensitivity of the circuit to variations.

In order to evaluate the response of the circuit subject to parasitic imperfections, we consider deviations from the assigned values for the phase delay of the PSs and the coupling coefficient of the CPs. Otherwise, the rest of the properties are assumed to be unperturbed. The errors are described as a normal distribution around the parameters' nominal values with varied standard deviations (hereafter σ) considered. In the Monte Carlo simulations, a population of 100 experiments is defined for which the parameter values are randomly generated.

3. RESULTS AND DISCUSSIONS

In a programmable photonic circuit, routing is the most prevalent functionality to be implemented, as it is used to interconnect all other functions. For simple routing, couplers will only be configured in either cross (coupling coefficient $\kappa = 1$) or bar state ($\kappa = 0$). In contrast with ordinary circuits, where routing is done through static waveguides, in a programmable circuit, the routing is done by the tunable couplers. As a result, there is much higher possibility for light to leak into adjacent paths and cause undesired interference within the circuit.

The couplers, which are used to create the actual route, are referred to as routing couplers (RCPs), and remained couplers in the mesh are the unused couplers (UCPs); UCPs are not involved in the routing. Further, under perfect operation conditions, their state does not affect the path shape. However, as we will see, their state does affect the function of the circuit in the presence of imperfections. Therefore, we define two different biasing schemes: setting all the UCPs in bar state or cross state. We refer to these biases as "normal bar" (NB) and "normal cross" (NC), respectively [Fig. 1(c)]. For the schematic demonstration of the unused and routing couplers, we have chosen the blue color for the UCPs and gray/orange color for the RCPs when they are in the bar/cross state, respectively.

A. Single Paths

Figure 2(a) shows a path (with $L_{\text{path}} = 6L_u$) routed through a seven-cell mesh, and Fig. 2(b) plots the transmission from the input to the output port for NB bias (red lines) and NC bias (green lines), with random variations in the couplings κ with $\sigma_k = 0.05\%, 0.4\%, 1.0\%$, and variations in the phase delays ϕ with $\sigma_\phi = 17°$. When the mesh is ideally programmed (black dashed lines), we expect that the length of the path will only contribute losses. However, as the graph for the NB bias shows, when random coupling variations increase, we see that levels of transmissions drop and significant ripples appear on the output spectrum. In fact, unwanted coupling will introduce additional losses because light is tapped out of the main path; further, it also introduces parasitic interference paths and even ring resonators. Although additional losses caused by unwanted couplings from the main path are inevitable, it is expected that proper programming of the unused couplers (using NC bias) suppresses parasitic interference paths and prevents ripples of the transmission response. As shown in Fig. 2(b), using NC bias can successfully compensate light accumulation in the mesh and suppress the formation of the coupled ring resonators in the mesh. As a result, the ripples of transmission have been suppressed.

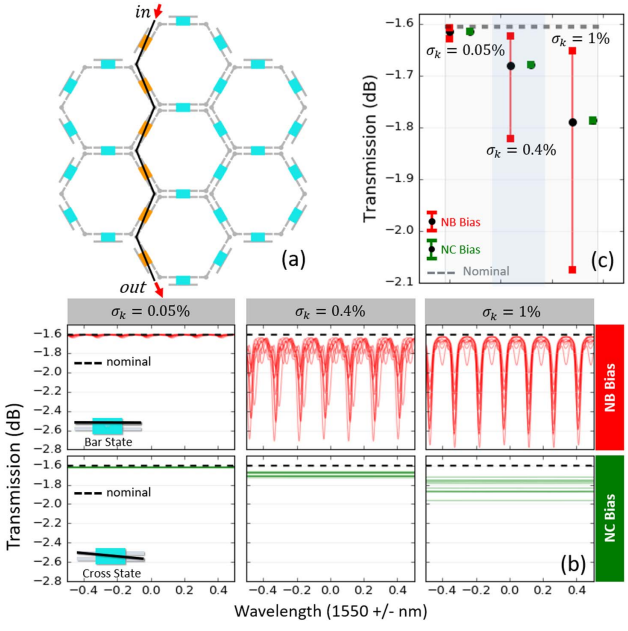

Fig. 2. (a) Schematic of a routed path (with $L_{\text{path}} = 10L_u$) within a seven-cell mesh. (b) Transmission spectra of the mesh for two types of biasing: normal bar (NB), where unused couplers are biased in the bar state (red curves), and normal cross (NC), where unused couplers are biased in the cross state (green curves). The results are plotted for $\sigma_k = 0.05\%$, 0.4%, and 1.0% from left to right. (c) Intensity spread analysis of the transmission in the output for random variations of $\sigma_k = 0.05\%$, 0.4%, and 1.0%. Red and green error bars correspond to the NB and NC biases.

To analyze the response of the programmed mesh for the NB and NC biases, we collected the 5%–95% intensity spread in the transmission spectra of Fig. 2(b) for 100 Monte Carlo simulations with the different random coupling variations of $\sigma_k = 0.05\%, 0.4\%, 1.0\%$, and plotted them as red (NB bias) and green (NC bias) error bars in Fig. 2(c). The [min, mean, max] points of the error bars are obtained by

$$\min = \min\{\min[T(\lambda)]_5, \ldots, \min[T(\lambda)]_{95}\}, \tag{1a}$$

$$\text{mean} = \text{mean}\{\text{mean}[T(\lambda)]_5, \ldots, \text{mean}[T(\lambda)]_{95}\}, \tag{1b}$$

$$\max = \max\{\max[T(\lambda)]_5, \ldots, \max[T(\lambda)]_{95}\}. \tag{1c}$$

The subscripts 5 and 95 indicate that we only considered the 5th–95th percentile of the samples, discarding the most extreme values. Comparing error bars clearly shows that NC bias considerably reduces the intensity spread of the transmission (>95%).

We performed this intensity spread analysis on a variety of simple and complex paths for NB and NC biases (Fig. 3). Similar to Fig. 2(c), error bars are plotted for three different values of σ_k and compared with the nominal response of the path (shown by black dashed lines). Each configuration is illustrated either above or below its corresponding intensity spread error bars. As seen, for NB bias, larger σ_k causes more intensity spread (larger ripples in spectrum) and losses, and complex paths with loops in their configuration (L, M, N) have error bars with a maximum transmission higher than the nominal values; in fact, effects of parasitic shortcuts (shorter paths with lower loss than the main path) are more prominent and can result in constructive interference of the output signal arriving through shortcuts. On the other side, for the NC bias, the effect of parasitic interference is almost eliminated for the simple paths; in addition, for the more complex paths, although this benefit diminishes, we still see a reduction of 50% in the intensity spread compared to NB bias.

It is worth noting that resonances are an artifact that only occurs in recirculating meshes. Forward-only meshes [10,14]

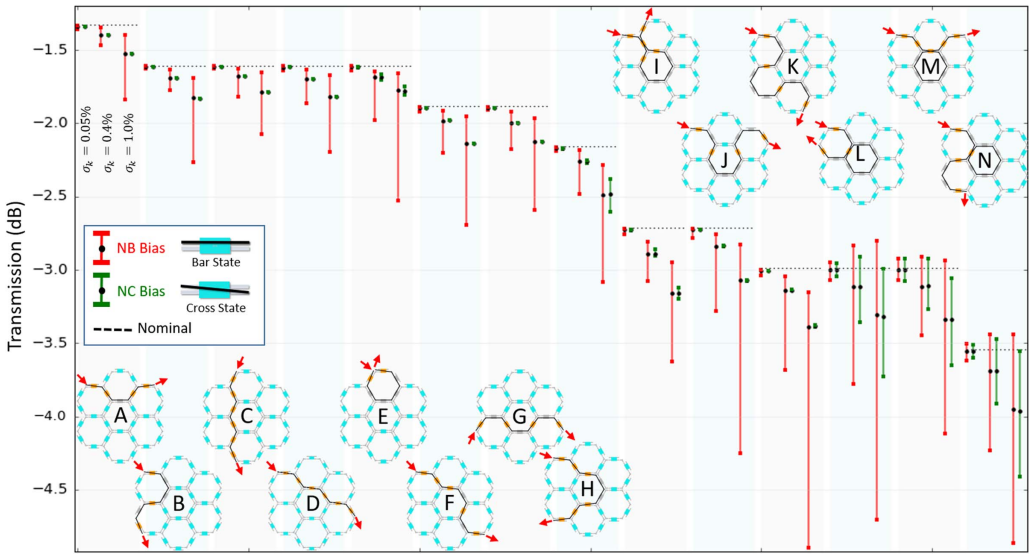

Fig. 3. Intensity spread analysis of different configurations of the seven-cell mesh to study both simple and complex paths. Blue couplers are in the bar (cross) state for the NB (NC) bias. Random variations of $\sigma_k = 0.05\%$, 0.4%, and 1.0% are chosen for the Monte Carlo simulations. Red and green error bars correspond to the NB and NC bias, respectively.

can also suffer from parasitics, but there we are only considering feed-forward interferences. Still, in the case of a single parasitic beam, this can still lead to a 10% intensity fluctuation when the parasitic beam carries only 1% of power. A second advantage of feed-forward meshes is that they are easier to control with simple minimizing/maximizing feedback loops [10], which can help to reduce the parasitics in real time.

B. Multipath Routing

The advantage of a programmable circuit is that we can implement multiple functions at the same time, connect multiple inputs to multiple outputs, and even use the tunable couplers as crossings to make intersecting paths. Of course, when there are imperfections in such scenarios, it is important that crosstalk between different paths is kept to a minimum. Figures 4(a) and 4(b) show the intensity spread of the transmission and crosstalk spectra of a mesh configured for the vertical and horizontal double-paths (A and C) and a multipath composed of them (B).

It is clear from Fig. 4 that putting the circuit in NC bias (green bars) eliminates parasitic shortcuts for all the cases, and their transmission intensity spread reaches 0 dB. This means that, similar to Fig. 2(b), all ports will have an almost flat transmission response without ripples. However, increasing σ_k will increase losses and reduce transmitted power, which is inevitable. In NB bias, the effect of parasitics is noticeable for the double-paths (A and C), while it has been reduced for the C configuration. The reason is that the C configuration has more couplers in the cross state, which breaks loops in the mesh and stops light accumulation inside of it. For the crosstalk, plotted in Fig. 4(b), increasing σ_k increases its value for all configurations for both NB and NC biases. It is also seen that outputs in A (O_1 and O_2) and C (O_3 and O_4) configurations have higher crosstalk compared with the B configuration.

C. Mach–Zehnder Interferometers

Mach–Zehnder interferometers (MZI) are the basis of all finite-impulse-response filters. The performance of a single MZI is a

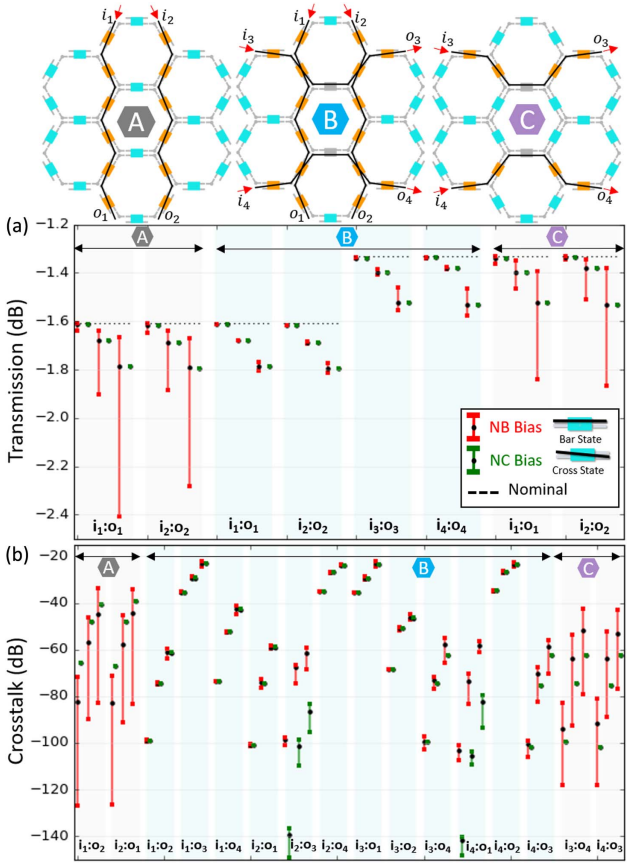

Fig. 4. Intensity spread analysis of the (a) transmission and (b) crosstalk of double- and multipaths. Similar to the Fig. 2(c), error bars are plotted for $\sigma_k = 0.05\%$, 0.4%, and 1.0%.

measure of how easily and accurately higher-order filters can be implemented. A simple MZI can also be easily evaluated for imperfections from the point of view of extinction ratio and absolute wavelength registration.

Figure 5(a) shows three different configured MZIs (A: $\Delta L = 6L_u$, B: $\Delta L = 4L_u$, C: $\Delta L = 10L_u$). The corresponding transmission responses of these three configurations are plotted in Fig. 5(b), where we have again used red and green curves for NB and NC biases. Here, to show the effect of NB and NC biases, 10 cycles of Monte Carlo simulations are used for $\sigma_k = 1\%$ and $\sigma_\phi = 17°$. Also, for simplicity, only one of the outputs (O_1) is shown (the other one, O_2, shows similar behavior). As seen, while the coupling errors mainly cause deterioration in the extinction ratio and weak appearance of other harmonics, the error in the phase shifters introduces a redshift or blueshift in the spectrum. Although phase shifter errors deteriorate the responses for NC and NB biases, NC bias shows better extinction ratios.

In order to quantify performance of the circuit for the selected MZI configurations, a correlation-based analysis has been performed using 100 cycles of Monte Carlo simulations; the results are shown in Fig. 5(c). Here, three pairs of coupling and phase variations (σ_k, σ_ϕ) have been selected: (0.05%, 17°); (1.0%, 17°); and (1.0%, 2°). For this analysis, the nominal response without perturbation is considered as the reference signal (R); for the perturbed responses (S), the correlation with the R [$\mathrm{Corr}(S,R)^2$] is calculated. The autocorrelation of the reference [$\mathrm{Corr}(R,R)^2$] has its maximum at the zero shift [$\mathrm{Corr}(R,R)^2|_{\Delta\lambda=0}$], and both correlation functions show small local maxima due to their periodic behavior. The closer the period of the two signals, the more similar these local maxima. The correlation graphs are also normalized with respect to the autocorrelation of S [$\mathrm{Corr}(S,S)^2$] and R [$\mathrm{Corr}(R,R)^2$]. In other words, the normalized correlation function can be read as

$$\widetilde{\mathrm{Corr}}(S,R)^2 = \frac{\mathrm{Corr}(S,R)^2}{\sqrt{\mathrm{Corr}(S,S)^2|_{\mathrm{MAX}} \cdot \mathrm{Corr}(R,R)^2|_{\mathrm{MAX}}}}. \quad (2)$$

The value $\widetilde{\mathrm{Corr}}(S,R)^2|_{\Delta\lambda=0}$ corresponding to the normalized correlation of S with R is an indicative value of the resemblance of the nominal and perturbed responses. At a shift wavelength of $\Delta\lambda_{\mathrm{MAX}}$, the normalized correlation curve of S has a maximum $\widetilde{\mathrm{Corr}}(S,R)^2|_{\mathrm{MAX}}$. This indicates that, on average, S has a $\Delta\lambda_{\mathrm{MAX}}$ shift as compared with R; if such a shift was absent (or unimportant depending on the application), the resemblance value of S and R would be $\widetilde{\mathrm{Corr}}(S,R)^2|_{\mathrm{MAX}}$. Figure 5(c) shows calculated values of $\widetilde{\mathrm{Corr}}(S,R)^2|_{\Delta\lambda=0}$, $\Delta\lambda_{\mathrm{MAX}}$, and $\widetilde{\mathrm{Corr}}(S,R)^2|_{\mathrm{MAX}}$ for the configured MZIs and different pairs of (σ_k, σ_ϕ), where we have used error bars to compare NB (red) and NC (green) biases. As seen, phase error, compared with coupling error, is the prominent factor, and, by reducing it to 2°, we can achieve acceptable resemblance with the nominal response. It is also seen that NC bias, unlike with the basic routing, does not improve the results for the MZI configurations.

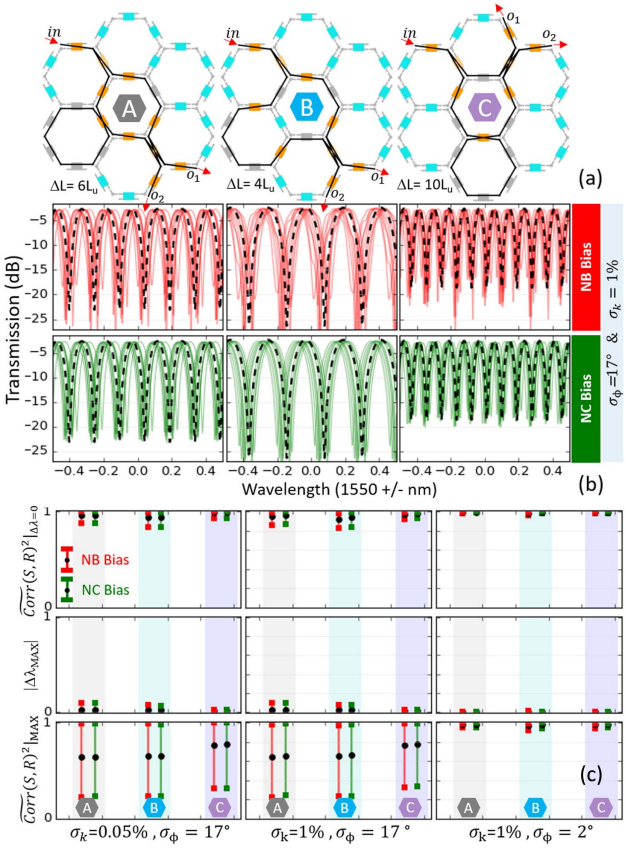

Fig. 5. (a) Schematic of the three different configured MZIs in the seven-cell hexagonal mesh (A: $\Delta L = 6L_u$, B: $\Delta L = 4L_u$, C: $\Delta L = 10L_u$). (b) Transmission response of the MZIs for NB (red) and NC (green) biases, where only 10 cycles of the Monte Carlo simulations have been plotted for better visibility. (c) Correlation-based analysis of the configured MZIs for (σ_k, σ_ϕ) pairs of (0.05%, 17°), (1.0%, 17°), and (1.0%, 2°).

D. Ring Resonators

Ring resonators, which are the building blocks of many silicon photonics filters, are susceptible to peak-splitting due to back-reflection. While we did not incorporate backreflection in the parasitic analysis (they are considered as a second type of parasitics), the hexagonal mesh allows for clockwise/counterclockwise coupling through the coupling between two adjacent rings, which are not originally designed to share any signal. This has a similar effect as backreflection or backcoupling in the tunable couplers. Figure 6(a) shows three configured ring resonators (A, B, C) in our chosen seven-cell hexagonal mesh. For the A and C configurations, rings are located in the center of the mesh; however, their bus waveguides are routed differently. For the B configuration, the ring is located near the boundary of the mesh, and its bus waveguide is created by a long and complex path. Transmission responses of these configurations for NB (red) and NC (green) biases with $\sigma_k = 1\%$ and $\sigma_\phi = 17°$ are plotted in Fig. 6(b), where 10 cycles of Monte Carlo simulations have been used. As expected, the phase errors mainly have caused wavelength shifts for all configurations and the coupling error affects the extinction ratio. However, complexity of the path in configuration B has created a larger extinction ratio.

We also have analyzed the performance of the ring resonators using the same correlation technique used for the MZI analysis. Figure 6(c) shows calculated values of

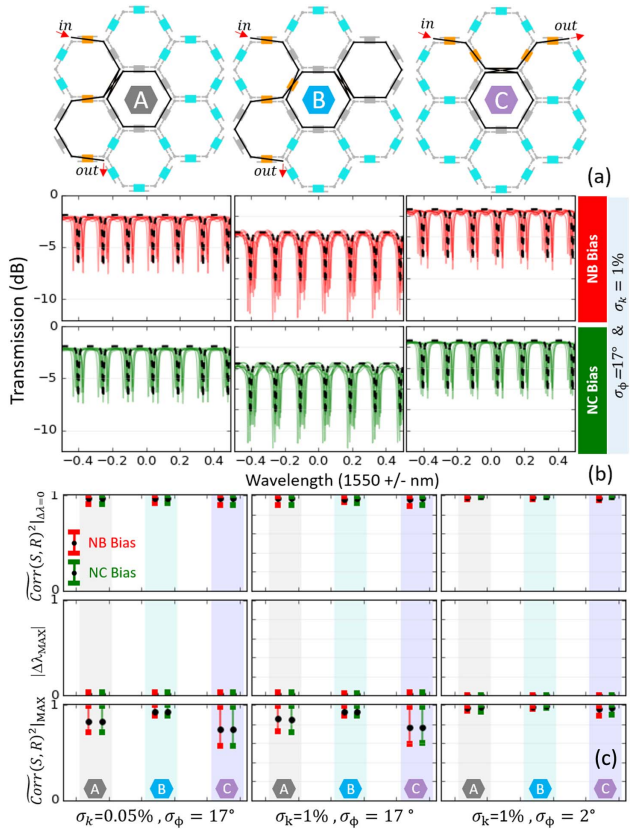

Fig. 6. (a) Schematic of three different configured ring resonators in the seven-cell hexagonal mesh. (b) Transmission response of the selected configurations for NB (red) and NC (green) biases, where 10 cycles of the Monte Carlo simulations have been used. (c) Correlation-based analysis of the configured ring resonators for (σ_k, σ_ϕ) pairs of (0.05%, 17°), (1.0%, 17°), and (1.0%, 2°).

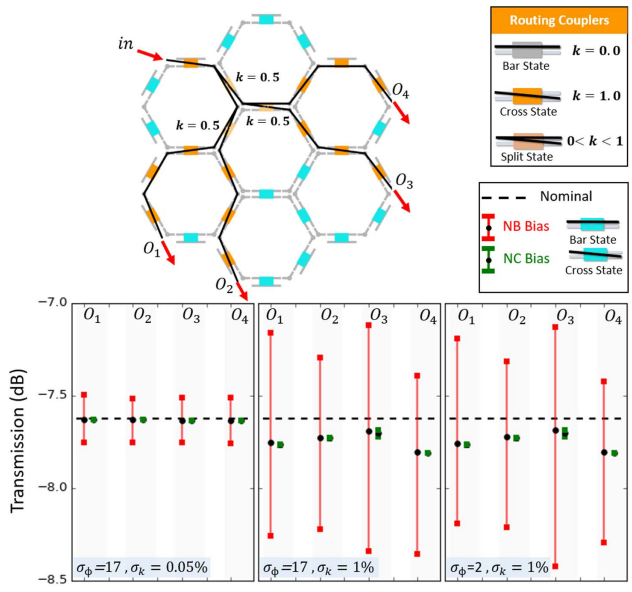

Fig. 7. Intensity spread analysis of a 1 × 4 splitter in the seven-cell hexagonal mesh. Red and green bars show NB and NC biases, respectively. Similar to Fig. 2(c), error bars are plotted for σ_k = 0.05%, 0.4%, and 1.0%. For NC bias, blue couplers are in the cross state (k = 1), while they are in the bar state (k = 0) for NB bias.

$\widetilde{Corr}(S,R)^2|_{\Delta\lambda=0}$, $\Delta\lambda_{MAX}$, and $\widetilde{Corr}(S,R)^2|_{MAX}$ for the configured resonators and different pairs of (σ_k, σ_ϕ). Similar to the MZIs, phase errors can considerably change the shape of the circuit response, and, by reducing σ_ϕ to 2°, we can achieve a resemblance of more than 90%. Another observation is that, although using NC bias cannot eliminate the effect of phase errors, selecting the ring close to the boundaries (configuration B) can significantly improve performance of the circuit. Comparing configurations A and C also shows that the routing of the path can also affect the response of the circuit even if the rings are in the same location.

E. Splitters and Power Distribution Networks

Another important configuration in programmable circuits is splitters, which can be used for multicasting or as a distribution network for an optical beam former. Here, we present an intensity spread analysis of a 1 × 4 (Fig. 7) and 1 × 16 (Fig. 8) splitter network. Similar to the previous cases, two biasing schemes (NB and NC biases) are compared, and random variations of σ_k = 0.05%, 0.4%, 1.0%, and σ_ϕ = 17° are applied to the couplings k and phase shifts ϕ, respectively.

As seen in Fig. 7, similar to the simple routing paths, the coupling error is the dominant factor that affects the power transmission. For NB bias, increasing σ_k from 0.05% to

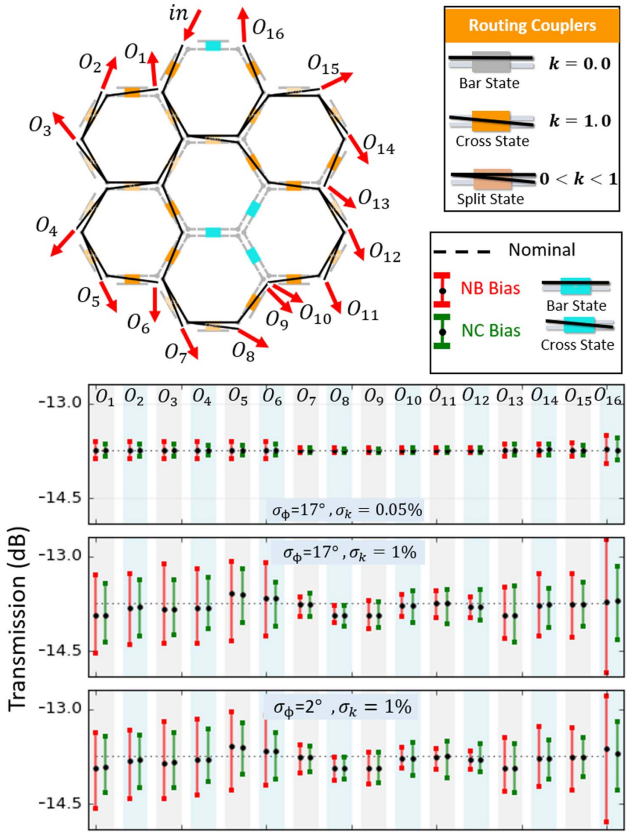

Fig. 8. Intensity spread analysis of a 1 × 16 splitter in a seven-cell hexagonal mesh. Red and green bars also show NB and NC biases, respectively. Similar to Fig. 2(c), error bars are plotted for σ_k = 0.05%, 0.4%, and 1.0%. For NC bias, blue couplers are in the cross state (k = 1), while they are in the bar state (k = 0) for the NB bias.

1.0% results in 0.25 dB to 1.8 dB power variation in the transmitted signals to the outputs. Also, higher transmissions are seen compared with their nominal response, indicating parasitic shortcuts, as discussed for the paths. However, applying NC bias successfully compensates the effect of unwanted interferences caused by parasitic couplers, and intensity spread reduces by more than 95%.

For the 1 × 16 splitter, almost all ports and coupler elements of the mesh are actively used; further, the circuit is operating at its full capacity. Hence, there is small room to compensate the effect of parasitics using unused couplers. This can be observed by comparing green (NC bias) and red (NB bias) error bars in Fig. 8. As seen, intensity spread reduction by the NC bias is less than 0.2 dB. Also, similar to the 1 × 4 beam splitter, parasitic shortcuts have increased power level of the transmitted signal. Another observation is lower intensity spread of the O_7 – O_{12} ports compared with the others (50% less).

F. Customized Biasing Schemes

As discussed above, by using NC bias, parasitic effects can be eliminated considerably for the paths and splitters. However, setting all of the unused couplers in the cross state is not the only solution for parasitic elimination. In fact, by proper programming of some of unused couplers, the same or better results can be achieved. To elaborate on this, transmission spread analyses of a single path ($\Delta L = 8L_u$) for the NB bias, NC bias, and three other customized biases are shown in Fig. 9, where $\sigma_k = 0.05\%$, 0.4%, and 1.0%. As seen, by programming only a few unused couplers, much better results can be achieved; for the biasing scheme of E, the transmission spread has been reduced by 95% for $\sigma_k = 0.1$. The importance of such optimization is in consuming lower energy to eliminate parasitic effects. Hence, for future studies, optimization of algorithms and strategies can be studied in more depth to find the optimum solutions for proper biasing of desired configurations.

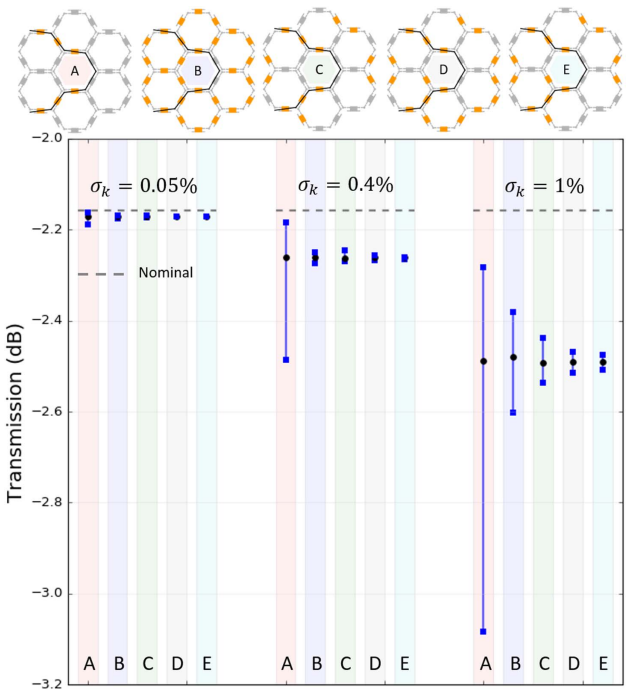

Fig. 9. Transmission spread analysis of a single path (with $\Delta L = 8L_u$) for different biasing schemes with $\sigma_k = 0.05\%$, 0.4%, and 1.0%.

4. CONCLUSION

Two biasing schemes for the unused couplers in a hexagonal seven-cell mesh are compared for their impact on different configurations of single paths, multipaths, ring resonators, MZIs, and splitters. In these schemes, the unused couplers are set either in the bar state (NB bias) or cross state (NC bias). Monte Carlo simulations show that NC bias considerably suppresses the effects of parasitics on the transmission response of the mesh for straight paths and becomes less effective for complex paths with loops. Transmission spread of the paths exponentially grows with increase of the coupling errors; further, it can vary from 0.03 dB ($\sigma_k = 0.05\%$) to 1.8 dB ($\sigma_k = 1.0\%$). Using less than four couplers out of six per cell more or less guarantees the possibility to compensate the parasitics using NC bias. Paths with loops in the center of the mesh are more vulnerable against parasitics compared with those with loops near edges of the mesh. Also, using custom optimized biasing, we have shown that it is also possible to eliminate parasitic effects with fewer unused couplers.

On the other hand, for ring resonators and MZIs in which the phase shifter's error is dominant and affects the depth of nulls, both biasing schemes have similar effects. However, selecting the ring near the edges of the mesh can improve correlation of the perturbed response with the ideal one. Moreover, the example of the 1 × 16 beam splitter shows that, although it is possible to use most of the mesh couplers to achieve a certain configuration, it limits our freedom to compensate parasitics by the remaining unused couplers.

It is important to realize that our compensation mechanism relies on shunting all the unused light to the edge of the circuit. When the mesh grows larger, there is less "edge" compared with "bulk." Therefore, a large mesh could benefit from "beam dumps" in different places inside the mesh (maybe even each cell), which could be activated by switches.

The use of switches could introduce another benefit: in these simulations, we used tunable couplers, which are controlled in a continuous way; in fact, in most locations they are used as switches in a cross or bar state. Using a mix of digital switches and tunable couplers in a mesh might help suppress parasitics, if the switches can have a better guaranteed extinction ratio.

Overall, we can say that more precise control results in lower parasitics. This requires good electronics, calibration, and control of other parasitics (electronic and thermal crosstalk). Incorporating control loops in a recirculating mesh (just like in feed-forward meshes) is also possible but not without additional tricks, such as the use of power monitors inside the mesh (e.g., CLIPPs [25]). Depending on the combinations of light paths in the mesh, we would require some form of labeling of the signals (e.g., with a frequency pilot tone), so we can know which light is inadvertently coupled to the wrong path [26]. As a main conclusion, we can state that recirculating meshes will suffer from parasitics, more than forward-only meshes, but that

overdimensioning the mesh and good biasing of the unused couplers can go a long way in suppressing unwanted resonances that these parasitic couplings will generate.

Funding. European Research Council (780283-MORPHIC); Horizon 2020 Framework Programme (725555-PhotonicSWARM).

Disclosures. The authors declare no conflicts of interest.

REFERENCES

1. L. Chen, E. Hall, L. Theogarajan, and J. Bowers, "Photonic switching for data center applications," IEEE Photon. J. **3**, 834–844 (2011).
2. L. Zhuang, C. G. H. Roeloffzen, M. Hoekman, K.-J. Boller, and A. J. Lowery, "Programmable photonic signal processor chip for radiofrequency applications," Optica **2**, 854–859 (2015).
3. A. Ribeiro, A. Ruocco, L. Vanacker, and W. Bogaerts, "Demonstration of a 4 × 4-port self-configuring universal linear optical component," in *Progress in Electromagnetics Research Symposium (PIERS)* (2016), Vol. **3**, pp. 3372–3375.
4. D. A. Miller, "Silicon photonics: meshing optics with applications," Nat. Photonics **11**, 403–404 (2017).
5. A. Annoni, E. Guglielmi, M. Carminati, G. Ferrari, M. Sampietro, D. A. Miller, A. Melloni, and F. Morichetti, "Unscrambling light—automatically undoing strong mixing between modes," Light Sci. Appl. **6**, e17110 (2017).
6. D. Pérez, I. Gasulla, and J. Capmany, "Toward programmable microwave photonics processors," J. Lightwave Technol. **36**, 519–532 (2018).
7. A. Peruzzo, A. Laing, A. Politi, T. Rudolph, and J. L. O'Brien, "Multimode quantum interference of photons in multiport integrated devices," Nat. Commun. **2**, 224 (2011).
8. B. J. Metcalf, N. Thomas-Peter, J. B. Spring, D. Kundys, M. A. Broome, P. C. Humphreys, X. M. Jin, M. Barbieri, W. Steven Kolthammer, J. C. Gates, B. J. Smith, N. K. Langford, P. G. Smith, and I. A. Walmsley, "Multiphoton quantum interference in a multiport integrated photonic device," Nat. Commun. **4**, 1356 (2013).
9. D. A. B. Miller, "Self-aligning universal beam coupler," Opt. Express **21**, 6360–6370 (2013).
10. D. A. B. Miller, "Self-configuring universal linear optical component (Invited)," Photon. Res. **1**, 1–15 (2013).
11. J. Carolan, C. Harrold, C. Sparrow, E. Martín-López, N. J. Russell, J. W. Silverstone, P. J. Shadbolt, N. Matsuda, M. Oguma, M. Itoh, G. D. Marshall, M. G. Thompson, J. C. Matthews, T. Hashimoto, J. L. O'Brien, and A. Laing, "Universal linear optics," Science **349**, 711–716 (2015).
12. D. A. B. Miller, "Perfect optics with imperfect components," Optica **2**, 747–750 (2015).
13. N. C. Harris, G. R. Steinbrecher, M. Prabhu, Y. Lahini, J. Mower, D. Bunandar, C. Chen, F. N. Wong, T. Baehr-Jones, M. Hochberg, S. Lloyd, and D. Englund, "Quantum transport simulations in a programmable nanophotonic processor," Nat. Photonics **11**, 447–452 (2017).
14. M. Reck, A. Zeilinger, H. J. Bernstein, and P. Bertani, "Experimental realization of any discrete unitary operator," Phys. Rev. Lett. **73**, 58–61 (1994).
15. N. C. Harris, J. Carolan, D. Bunandar, M. Prabhu, M. Hochberg, T. Baehr-Jones, M. L. Fanto, A. M. Smith, C. C. Tison, P. M. Alsing, and D. Englund, "Linear programmable nanophotonic processors," Optica **5**, 1623–1631 (2018).
16. W. R. Clements, P. C. Humphreys, B. J. Metcalf, W. S. Kolthammer, and I. A. Walsmley, "Optimal design for universal multiport interferometers," Optica **3**, 1460–1465 (2016).
17. D. Perez, I. Gasulla, F. J. Fraile, L. Crudgington, D. J. Thomson, A. Z. Khokhar, K. Li, W. Cao, G. Z. Mashanovich, and J. Capmany, "Silicon photonics rectangular universal interferometer," Laser Photon. Rev. **11**, 1700219 (2017).
18. S. Pai, B. Bartlett, O. Solgaard, and D. A. Miller, "Matrix optimization on universal unitary photonic devices," Phys. Rev. Appl. **11**, 064044 (2019).
19. D. Pérez, I. Gasulla, J. Capmany, and R. A. Soref, "Reconfigurable lattice mesh designs for programmable photonic processors," Opt. Express **24**, 12093–12106 (2016).
20. D. Pérez, I. Gasulla, L. Crudgington, D. J. Thomson, A. Z. Khokhar, K. Li, W. Cao, G. Z. Mashanovich, and J. Capmany, "Multipurpose silicon photonics signal processor core," Nat. Commun. **8**, 636 (2017).
21. D. Pérez, I. Gasulla, and J. Capmany, "Programmable multifunctional integrated nanophotonics," Nanophotonics **7**, 1351–1371 (2018).
22. D. Pérez and J. Capmany, "Scalable analysis for arbitrary photonic integrated waveguide meshes," Optica **6**, 19–27 (2019).
23. A. Li, T. Van Vaerenbergh, P. De Heyn, P. Bienstman, and W. Bogaerts, "Backscattering in silicon microring resonators: a quantitative analysis," Laser Photon. Rev. **10**, 420–431 (2016).
24. W. Bogaerts, M. Fiers, M. Sivilotti, and P. Dumon, "The IPKISS photonic design framework," in *Optical Fiber Communications Conference and Exhibition (OFC)* (2016), pp. 1–3.
25. F. Morichetti, S. Grillanda, M. Carminati, G. Ferrari, M. Sampietro, M. J. Strain, M. Sorel, and A. Melloni, "Non-invasive on-chip light observation by contactless waveguide conductivity monitoring," IEEE J. Sel. Top. Quantum Electron. **20**, 292–301 (2014).
26. D. Oliveira, M. D. Aguiar, M. Milanizadeh, E. Guglielmi, F. Zanetto, G. Ferrari, M. Sampietro, F. Morichetti, and A. Melloni, "Automatic tuning of silicon photonics microring filter array for hitless reconfigurable add–drop," J. Lightwave Technol. **37**, 3939–3947 (2019).